Boron isotope compositions of coexisting kornerupine and tourmaline in high-grade metabasic rocks: an example from Akarui Point, Lützow-Holm Complex, East Antarctica

Tetsuo KAWAKAMI* and Simon L. HARLEY**

*Department of Geology and Mineralogy, Graduate School of Science, Kyoto University, Kyoto 606-8502, Japan
**School of GeoSciences, The University of Edinburgh, Edinburgh EH9 3FE, UK

Boron isotope compositions were measured in kornerupine and tourmaline from lenses consisting primarily of kornerupine, plagioclase and corundum. The lenses occur within hornblende-gneiss or along the boundary between this gneiss and an amphibolite lens at Akarui Point in the Lützow-Holm Complex, Prince Olav Coast, East Antarctica. The peak metamorphic conditions have been estimated to be ~ 800-900 °C and ~ 8-11 kbar. The $\delta^{11}B$ compositions of kornerupine, which is interpreted to have been a stable phase at the metamorphic peak, are -11.6 ± 0.4 to -7.8 ± 0.5‰ and -9.8 ± 0.3 to -6.1 ± 0.2‰ in two different samples. Grains of prograde tourmaline included in kornerupine and corundum yielded $\delta^{11}B = -2.1 \pm 0.3$ to $+0.6 \pm 0.3$‰, and the secondary tourmaline replacing kornerupine yielded $\delta^{11}B = -4.6 \pm 0.2$ to -3.7 ± 0.2‰. Therefore, the isotopic fractionation between kornerupine and tourmaline, $\Delta^{11}B_{Tur\text{-}Krn}$ ($= \delta^{11}B_{Tur} - \delta^{11}B_{Krn}$), of the average prograde tourmaline and average host kornerupine is $+6.7 \pm 1.5$‰, which is interpreted to indicate isotopic equilibrium at the metamorphic peak on the basis of previous studies of isotope fractionation between tourmaline and minerals of the kornerupine-prismatine series. The $\delta^{11}B$ values obtained on prograde tourmaline are between whole rock $\delta^{11}B$ of MORB and mantle rocks and of some sedimentary rocks, and are similar to the $\delta^{11}B$ of blackwall tourmalines that crystallized during the decompression stage following high-pressure metamorphism. We infer that the syn-metamorphic B-bearing fluid present in the kornerupine-plagioclase-corundum lens is likely sourced from a mixture of sedimentary, mafic and ultramafic lithologies in a subduction setting. The metabasic and meta-ultramafic lenses found in Akarui Point could be interpreted as the remnant of mixing zone of Ediacaran to Cambrian subduction channel.

Keywords: Boron isotope, Metamorphic fluid, Tourmaline, Continental collision, Lower crust

INTRODUCTION

Boron is an incompatible element present in trace amount in oceanic sediments (<180 ppm), mafic igneous rocks (<35 ppm) and altered oceanic crust (<280 ppm) (Leeman and Sisson, 1996). Consequently, unusual concentrations of B, such as tourmaline aggregates in metamorphic rocks, are considered evidence for B-bearing fluid infiltration (e.g., Kawakami, 2001; Kawakami et al., 2008; Marschall et al., 2009; Kawakami et al., 2019). Tourmaline becomes unstable in granulite facies conditions depending on bulk composition of the host rock (Kawakami, 2001; Dutrow and Henry, 2011), and instead, kornerupine becomes stable in high-pressure (high-*P*) conditions above ~ 0.5 GPa (Robbins and Yoder, 1962; Krosse, 1995; Grew, 1996; Werding and Schreyer, 1996). Kornerupine sensu stricto and its B-dominant analogue prismatine, both (□, Mg, Fe)(Al, Mg, Fe)$_9$(Si, Al, B)$_5$O$_{21}$(OH, F), have been reported from at least 84 localities worldwide as of 2017 in upper amphibolite- and granulite-facies rocks (Grew, 1996; Grew et al., 2017). Accumulation of kornerupine can, therefore, be a tracer of B-bearing fluids under high-*P* conditions as well.

Boron isotope composition of borosilicates is potentially a powerful tool to constrain the nature of infiltrated fluid even in high-temperature (high-*T*) metamorphic rocks. To date, only one such B-isotope study has been carried out on kornerupine-prismatine-bearing borosili-

doi:10.2465/jmps.230131b
T. Kawakami, t-kawakami@kueps.kyoto-u.ac.jp Corresponding author

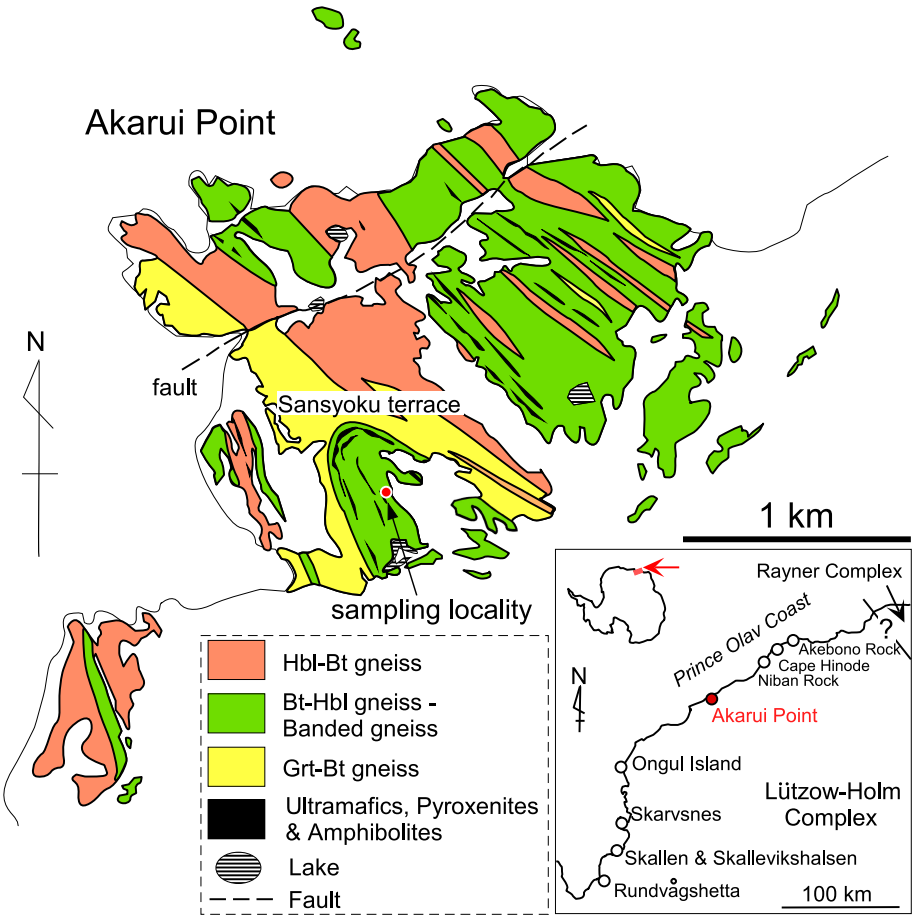

Figure 1. Geological map of the Akarui Point showing the sampling locality (modified after Yanai et al., 1984). Inset shows the location of Akarui Point in the Prince Olav Coast, and a red arrow indicates the location of the Lützow-Holm Complex in Antarctica.

cate assemblages (MacGregor et al., 2013), and more such studies are needed to better understand the systematics of B isotope behavior in the lower crust.

Metamorphic tourmaline and tourmaline accumulations (blackwalls) in subduction zone settings have been extensively studied recently to understand the fluid-rock interaction in the mixing zone of subduction zones (Nakano and Nakamura, 2001; Bebout and Nakamura, 2003; Altherr et al., 2004; Marschall et al., 2006, 2008, 2009; Marocchi et al., 2011; Van Hinsberg et al., 2011). Fluids released from subducting sedimentary rocks and altered oceanic crust are understood to be the important source of B in these cases. In contrast, tourmaline accumulations associated with mafic and ultramafic rocks in collision settings could be interpreted as metamorphosed blackwalls or the result of fluid rock interaction during collision metamorphism. In this study, we describe an unusual kornerupine-plagioclase-corundum (Krn-Pl-Crn) lens associated with hornblende-gneiss and amphibolite at Akarui Point, Lützow-Holm Complex (LHC), Prince Olav Coast, East Antarctica in order to better understand the behavior of B in a zone of mixing in a collision setting. Mineral abbreviations follow Warr (2021).

GEOLOGICAL SETTING

The LHC is a Cambrian orogenic belt bounded by the Late Proterozoic to Cambrian Rayner Complex to the east and by the Late Proterozoic to Early Palaeozoic Yamato-Belgica Complex to the west (Shiraishi et al., 1994; Satish-Kumar et al., 2008). Based on mapping using index minerals, the metamorphic grade of the complex has been shown to increase progressively from the upper amphibolite facies on the Prince Olav Coast through a transitional zone to the granulite facies in Lützow-Holm Bay (Hiroi et al., 1991) (Fig. 1). A thermal axis of maximum peak metamorphic temperature is estimated to lie in southern Lützow-Holm Bay near Rundvågshetta (Motoyoshi and Ishikawa, 1997). Ultrahigh-temperature (UH*T*) metamorphism of about 1000 °C, 1.1 GPa and subsequent isothermal decompression are reported from Rundvågshetta (Ishikawa et al., 1994; Yoshimura et al., 2008). The complex experienced a typical clockwise *P*-*T* path (Hiroi et al., 1983, 1991; Kawakami and Motoyoshi, 2004), and recent studies support isothermal decompression starting from kyanite stability field (Iwamura et al., 2013; Kawakami et al., 2016). The *P*-*T* estimates by Zr-in-rutile ther-

mometry applied to inclusion rutile grains in garnet reveal that similar *P*–*T* conditions of ~ 830–850 °C at ~ 1.1 GPa are widely attained from Akarui Point to Skallen (Suzuki and Kawakami, 2019). This suggests that the transitional zone defined by the metamorphic field mapping using matrix mineral assemblage of mafic to intermediate gneisses is equivalent to the granulite facies zone.

In the amphibolite facies zone at Cape Hinode. ~ 960 Ma exotic block is found and termed as 'Hinode Block' (Shiraishi et al., 1994; Dunkley et al., 2020). Recently, high-grade metamorphism at ~ 990 to ~ 930 Ma is detected also from Niban Rock and Akebono Rock (Kitano et al., 2021; Baba et al., 2022), while Late Proterozoic to Cambrian metamorphic age (~ 600–520 Ma), which is widely recorded in metamorphic rocks of the surrounding LHC including Akarui Point, is not detected by U-Pb zircon dating (Kitano et al., 2021). Mori et al. (2023) reports traces of Cambrian metamorphism from Nibannishi rock of Niban Rock using electron microprobe U-Th-Pb monazite dating. In spite of above-mentioned recent progress, the geological boundaries of the Hinode Block and its relationship to the surrounding LHC remain unresolved (Baba et al., 2022).

Akarui Point is one of the nunataks in the 'transitional zone' on the Prince Olav Coast (Fig. 1, Hiroi et al., 1991). Dominant rock types are Bt-Hbl, Hbl-Bt, and Grt-Bt gneisses, with subordinate ultramafic rocks and pyroxene gneiss as lenses mainly enclosed in the Bt-Hbl gneiss. The Bt-Hbl and Hbl-Bt gneisses are locally migmatitic and grade into one another. Relict kyanite occurs as inclusions in garnet and plagioclase in the Grt-Bt gneiss (Hiroi et al., 1983). Orthopyroxene is one of the main constituent minerals in the ultramafic granulite and pyroxene gneiss (Yanai et al., 1984). Granites and pegmatitic veins with pinkish K-feldspar intrude discordantly to the foliation of metamorphic rocks (Yanai et al., 1984). A recent study reports peak *P*–*T* conditions of 834 ± 4 °C and ~ 1.1 GPa constrained by using the minerals included in garnet from the pelitic gneiss from Akarui Point (Suzuki and Kawakami, 2019). Iwamura et al. (2013) obtained slightly higher *P*–*T* estimate of ~ 900 °C and 1.1–1.2 GPa from a mafic granulite. Reintegration of lamellae in alkali-feldspar from the matrix of a sillimanite-biotite-garnet gneiss also gives temperature estimate of 825–900 °C (Nakamura et al., 2014). This peak metamorphic *P*–*T* condition is followed by decompression into the andalusite stability field (Kawakami et al., 2008).

ANALYTICAL SETTINGS

Quantitative analyses of kornerupine and tourmaline were performed by a JEOL JXA-8105 superprobe at Department of Geology and Mineralogy, Kyoto University, Japan. Analytical conditions for quantitative analyses were 15.0 kV acceleration voltage, 10 nA beam current, and 3 μm beam diameter. The counting time for the peak and backgrounds were 30 and 15 s for Cl, 60 and 30 s for F, and 10 and 5 s for other elements. Natural and synthetic minerals were used as standards and the ZAF correction was applied.

Boron isotopic compositions and B concentration of kornerupine and tourmaline were determined in situ by secondary ionization mass spectroscopy (SIMS) on the Cameca ims1270 instrument at the Edinburgh Ion Microprobe Facility following procedures similar to those of Grew et al. (2015). Operating conditions for tourmalines were 5.4 nA primary beam current of $^{16}O^-$ ions at a primary voltage 17.5 kV, producing an analytical spot size of ~ 10 × 15 μm. Following pre-sputter of 60 seconds, ^{11}B and ^{10}B signals were recorded in 20 cycles of 2 and 8 seconds, respectively, using a single electron multiplier detector with a dead time of 51 seconds. Typical count rates were 6.2×10^5 and 1.7×10^5 cps/nA/wt% B_2O_3, respectively. A mass resolution of 3100 (m/Δm at 5% peak width) was used to avoid interference of ^{10}BH, ^{9}BeH, and $^{9}BeH_2$ molecular species. No energy filtering was applied. Internal precision of the analyses was generally <0.3‰ (1σ). Drift in the $^{11}B/^{10}B$ ratio was minor, and the average for all drift-corrected measurements with the dravite standard gave 1σ uncertainty of 0.5‰. Standards used for tourmaline were elbaite 98144 ($\delta^{11}B_{SRM951} = -10.5‰$), schorl 112566 ($\delta^{11}B_{SRM951} = -12.5‰$) and dravite 108796 ($\delta^{11}B_{SRM951} = -6.6‰$), previously analyzed using thermal ionization mass spectrometry (TIMS) by Leeman and Tonarini (2001). Standards used for kornerupine/prismatine were prismatine 112233 ($\delta^{11}B_{SRM951} = -10.8‰$; Leeman and Tonarini, 2001) and two Larsemann Hills prismatines (Seal Cove: $\delta^{11}B_{SRM951} = -15.8‰$; and Stornes: $\delta^{11}B_{SRM951} = -13.7‰$) analyzed by TIMS (Samuele Agostini, personal communication) and reported in MacGregor et al. (2013).

During the analytical sequence, analyses of unknowns were bracketed with standard analyses to detect offset and drift. The analytical results were corrected for offsets using recommended values of standards and compositional correction was additionally made for tourmaline. Matrix-dependent mass fractionation in tourmaline was moderate: elbaite 98114 was offset by +1.9 ± 1.8‰ (1σ, $n = 4$) from the TIMS value (Leeman and Tonarini, 2001); schorl 112566 by +1.8 ± 0.7‰ (1σ, $n = 3$) and dravite 108796 by −0.1 ± 0.6‰ (1σ, $n = 6$). On this basis the analytical reproducibility is estimated to be better than 0.6‰ for analyses referenced principally to the dravite standard. The compositional correction made for the dravite-rich

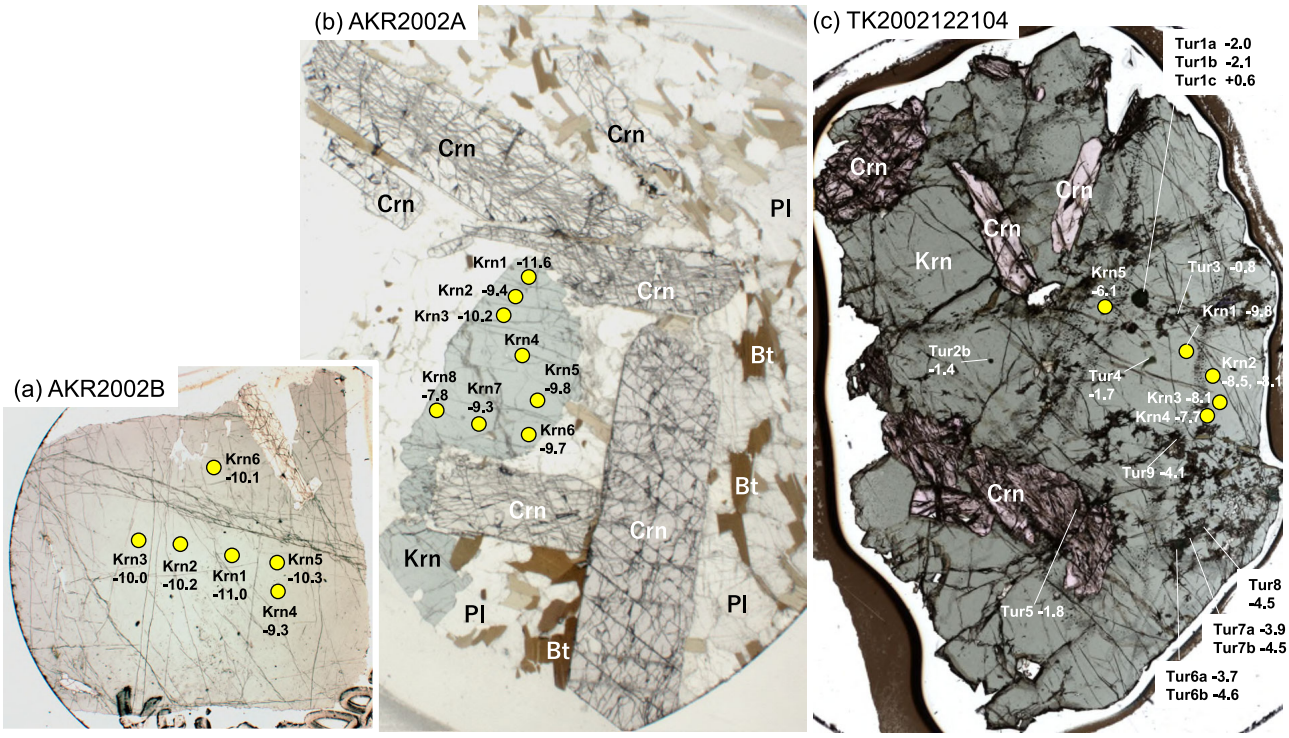

Figure 2. Photomicrograph of thin sections (plane polarized light) of samples (a) AKR2002B, (b) AKR2002A, and (c) TK2002122401 with analysis points and results of the in situ B isotopic measurements. Points labelled with 'Krn' represent analysis points for kornerupine and those labelled with 'Tur' represent analysis points for tourmaline. Numbers accompanied with analysis point numbers are $\delta^{11}B$ values determined in this study.

tourmalines analyzed in this study was only +0.1‰. Prismatines were referenced against the Seal Cove standard bracketing sets of 4–6 sample analyses, with instrumental mass fractionation (offset) correction applied based on the Seal Cove prismatine bracketing results.

Following the usual conventions, B isotope compositions are expressed as per mil deviation from the standard SRM951 boric acid in delta notation: $\delta^{11}B$ {= [($^{11}B/^{10}B)_{sample}/(^{11}B/^{10}B)_{NIST951} - 1$] * 1000}, using a value of $^{11}B/^{10}B = 4.0437$ for SRM951 (Catanzaro et al., 1970). Distribution of B isotopes between two minerals A and B is expressed as $\Delta^{11}B_{A\text{-}B}$ (= $\delta^{11}B_A - \delta^{11}B_B$).

SAMPLE DESCRIPTION

The Krn–Pl–Crn lenses in the Akarui Point are developed in a Hbl–Bt gneiss and also found between an amphibolite lens and the Hbl–Bt gneiss. Sample description is briefly summarized below based on Kawakami et al. (2008). Samples analyzed in this study are two Krn–Pl–Crn–bearing samples (AKR2002 and TK2002122104; Fig. 2) collected from an irregularly–shaped lens, roughly 50–60 cm across and surrounded by hornblende gneiss. Constituent minerals of the lens are coarser–grained than those in the surrounding hornblende gneiss. Kornerupine (X_{Mg} = 0.79–0.82) forms euhedral prisms up to 4 cm in diameter and 10 cm in length. In addition to kornerupine, the lens consists of euhedral corundum (Cr_2O_3 = 0.22–0.34 wt%) forming tabular crystals up to 3 cm in diameter, biotite (X_{Mg} = 0.79–0.82) as flakes 1–5 mm across, and plagioclase (An66–84). The kornerupine and coexisting corundum enclose euhedral to xenomorphic grains of greenish tourmaline (X_{Mg} = 0.82–0.83) in TK2002122104. These tourmaline inclusions are interpreted to have formed prior to or simultaneously with kornerupine and corundum and thus are considered to be prograde. Kornerupine is partly replaced along grain rims and cracks to secondary tourmaline (X_{Mg} = 0.79–0.85), corundum, andalusite and magnesite, a feature previously attributed to reaction with a retrograde CO_2–H_2O fluid (Kawakami et al., 2008). The microstructure of secondary tourmaline is fibrous or matted.

RESULTS OF BORON ISOTOPE ANALYSES

Analysis points for the in situ B isotopic measurements are shown in Figure 2. Mineral analyses together with B isotope data are summarized in Table 1 for kornerupine and Table 2 for tourmaline. The $\delta^{11}B$ values {= [($^{11}B/^{10}B)_{sample}/(^{11}B/^{10}B)_{NIST951} - 1$] * 1000} of kornerupine were −11.6 ± 0.4 to −7.8 ± 0.5‰ in sample AKR2002 and −9.8 ± 0.3 to

Table 1. Summary of major element and B isotope compositions of kornerupine

Sample name	AKR2002B					
Spot no.	Krn1	Krn2	Krn3	Krn4	Krn5	Krn6
Comment	Core					
SiO_2	29.62	29.91	29.60	29.59	30.14	29.60
TiO_2	0.28	0.17	0.14	0.00	0.00	0.25
Al_2O_3	44.19	44.55	43.55	43.65	43.75	43.77
Cr_2O_3	0.13	0.12	0.11	0.15	0.07	0.19
B_2O_3 (analyzed)	1.91	1.87	1.97	2.01	2.01	1.92
FeO	6.70	6.91	6.50	6.86	7.06	6.87
MnO	0.13	0.37	0.28	0.33	0.25	0.23
MgO	15.28	15.31	15.67	15.38	15.67	15.63
CaO	0.07	0.09	0.10	0.05	0.09	0.07
BaO	0.14	0.05	0.02	0.07	0.00	0.00
Na_2O	0.05	0.02	0.06	0.05	0.06	0.07
K_2O	0.01	0.00	0.00	0.00	0.01	0.00
F	0.01	0.00	0.00	0.00	0.00	0.00
Cl	0.00	0.01	0.01	0.01	0.00	0.00
-O≡F	0.00	0.00	0.00	0.00	0.00	0.00
-O≡Cl	0.00	0.00	0.00	0.00	0.00	0.00
H_2O calc	1.19	1.20	1.19	1.19	1.20	1.20
Total	99.70	100.57	99.20	99.32	100.29	99.79
Number of O	21.5	21.5	21.5	21.5	21.5	21.5
Si	3.71	3.72	3.73	3.72	3.76	3.71
Ti	0.03	0.02	0.01	0.00	0.00	0.02
Al	6.53	6.53	6.46	6.48	6.43	6.47
Cr	0.01	0.01	0.01	0.01	0.01	0.02
B	0.41	0.40	0.43	0.44	0.43	0.42
Fe	0.70	0.72	0.68	0.72	0.74	0.72
Mn	0.01	0.04	0.03	0.03	0.03	0.02
Mg	2.85	2.84	2.94	2.89	2.91	2.92
Ca	0.01	0.01	0.01	0.01	0.01	0.01
Ba	0.01	0.00	0.00	0.00	0.00	0.00
Ni	0.00	0.00	0.00	0.00	0.00	0.00
Na	0.01	0.00	0.01	0.01	0.01	0.02
K	0.00	0.00	0.00	0.00	0.00	0.00
F	0.00	0.00	0.00	0.00	0.00	0.00
Cl	0.00	0.00	0.00	0.00	0.00	0.00
OH	1.00	1.00	1.00	1.00	1.00	1.00
Total cation	14.29	14.29	14.32	14.32	14.32	14.32
Mg/(Fe + Mg)	0.80	0.80	0.81	0.80	0.80	0.80
$\delta^{11}B_{NIST951}$‰	−11.0	−10.2	−10.0	−9.4	−10.3	−10.1
±1σ‰	0.46	0.37	0.33	0.29	0.35	0.49

n.d., not determined. All Fe as FeO.

−6.1 ± 0.2‰ in sample TK2002122104 (Fig. 3). In spite of the observed variation, there is no evidence for core to rim zoning in $\delta^{11}B$ in the three kornerupine grains analyzed (Fig. 2). The prograde tourmalines found as inclusions in kornerupine in sample TK2002122104 yielded −2.1 ± 0.3 to −2.0 ± 0.3‰ in their cores and +0.6 ± 0.3‰ on their rims, and that in corundum yielded similar value of −1.8 ± 0.2‰. The $\delta^{11}B$ values of prograde tourmaline are statistically different from those of secondary tourmaline, which range from −4.6 ± 0.2 to −3.7 ± 0.2‰ (Fig. 3).

DISCUSSION

The Krn–Pl–Crn lens has a high B content as suggested by

Table 1. (Continued-1)

Sample name	AKR2002A							
Spot no.	Krn1	Krn2	Krn3	Krn4	Krn5	Krn6	Krn7	Krn8
Comment	Rim					Rim		
SiO_2	29.25	29.27	29.74	29.63	29.70	29.80	29.44	29.66
TiO_2	0.28	0.17	0.14	0.20	0.06	0.00	0.06	0.00
Al_2O_3	43.97	44.29	43.16	44.07	43.49	43.57	43.62	43.82
Cr_2O_3	0.15	0.10	0.18	0.15	0.10	0.14	0.03	0.15
B_2O_3 (analyzed)	1.41	1.47	1.57	n.d.	1.63	1.51	1.49	1.41
FeO	7.16	7.38	6.62	6.81	6.64	6.56	6.35	6.36
MnO	0.30	0.25	0.34	0.17	0.35	0.17	0.27	0.31
MgO	15.76	15.86	15.58	15.89	15.72	15.64	15.76	15.78
CaO	0.10	0.03	0.02	0.08	0.09	0.05	0.07	0.07
BaO	0.00	0.00	0.00	0.00	0.00	0.00	0.01	0.07
Na_2O	0.05	0.07	0.06	0.07	0.06	0.08	0.04	0.05
K_2O	0.03	0.00	0.00	0.00	0.01	0.00	0.00	0.00
F	0.07	0.00	0.00	0.01	0.00	0.00	0.03	0.04
Cl	0.01	0.01	0.00	0.01	0.00	0.01	0.01	0.00
-O≡F	0.03	0.00	0.00	0.00	0.00	0.00	0.01	0.02
-O≡Cl	0.00	0.00	0.00	0.00	0.00	0.00	0.00	0.00
H_2O calc	1.15	1.19	1.18	1.16	1.19	1.18	1.16	1.16
Total	99.64	100.08	98.58	98.24	99.03	98.71	98.33	98.88
Number of O	21.5	21.5	21.5	21.5	21.5	21.5	21.5	21.5
Si	3.69	3.68	3.77	3.81	3.75	3.77	3.74	3.75
Ti	0.03	0.02	0.01	0.02	0.01	0.00	0.01	0.00
Al	6.54	6.56	6.46	6.67	6.48	6.50	6.53	6.54
Cr	0.01	0.01	0.02	0.02	0.01	0.01	0.00	0.02
B	0.31	0.32	0.34	n.d.	0.36	0.33	0.33	0.31
Fe	0.76	0.78	0.70	0.73	0.70	0.69	0.68	0.67
Mn	0.03	0.03	0.04	0.02	0.04	0.02	0.03	0.03
Mg	2.96	2.97	2.95	3.04	2.96	2.95	2.99	2.98
Ca	0.01	0.00	0.00	0.01	0.01	0.01	0.01	0.01
Ba	0.00	0.00	0.00	0.00	0.00	0.00	0.00	0.00
Ni	0.00	0.00	0.00	0.00	0.00	0.00	0.00	0.00
Na	0.01	0.02	0.02	0.02	0.01	0.02	0.01	0.01
K	0.00	0.00	0.00	0.00	0.00	0.00	0.00	0.00
F	0.03	0.00	0.00	0.00	0.00	0.00	0.01	0.02
Cl	0.00	0.00	0.00	0.00	0.00	0.00	0.00	0.00
OH	0.97	1.00	1.00	0.99	1.00	1.00	0.99	0.98
Total cation	14.36	14.37	14.31	14.34	14.33	14.31	14.32	14.32
Mg/(Fe + Mg)	0.80	0.79	0.81	0.81	0.81	0.81	0.82	0.82
$\delta^{11}B_{NIST951}$‰	−11.6	−9.4	−10.2	n.d.	−9.8	−9.7	−9.3	−7.8
±1σ‰	0.37	0.37	0.53	n.d.	0.31	0.40	0.38	0.46

n.d., not determined. All Fe as FeO.

the presence of large kornerupine crystals (up to 4 cm in diameter, ~ 1.9–2.0 wt% B_2O_3) as a major constituent mineral. Because B is highly incompatible and B concentrations in mafic and ultramafic rocks are generally low, the Krn–Pl–Crn lens present in mafic lithologies at Akarui Point is likely a product of interaction between B-bearing fluid and the host rock. Kawakami et al. (2008) proposed two possible scenarios for introducing B to form the Krn–Pl–Crn lenses: (1) Boron infiltration into the lens was syn-metamorphic facilitated through prograde dehydration of muscovite in surrounding metasediments. (2) Boron addition occurred prior to peak metamorphism through lower-temperature hydrothermal alteration of the mafic and ultramafic protoliths by seawater. These scenarios are tested

Table 1. (Continued-2)

Sample name	TK2002122104				
Spot no.	Krn1	Krn2	Krn3	Krn4	Krn5
Comment					
SiO_2	29.70	29.95	30.16	29.80	30.72
TiO_2	0.17	0.08	0.00	0.06	0.00
Al_2O_3	43.54	43.01	43.45	44.27	42.44
Cr_2O_3	0.22	0.13	0.15	0.11	0.16
B_2O_3 (analyzed)	1.56	1.61	1.63	1.89	2.06
FeO	6.97	6.16	6.84	6.64	6.65
MnO	0.18	0.21	0.20	0.38	0.27
MgO	15.48	15.35	15.42	15.19	15.24
CaO	0.10	0.10	0.04	0.07	0.06
BaO	0.04	0.04	0.00	0.07	0.04
Na_2O	0.01	0.07	0.03	0.01	0.05
K_2O	0.00	0.00	0.01	0.00	0.00
F	0.00	0.02	0.00	0.08	0.00
Cl	0.01	0.00	0.01	0.01	0.01
-O≡F	0.00	0.01	0.00	0.03	0.00
-O≡Cl	0.00	0.00	0.00	0.00	0.00
H_2O calc	1.18	1.16	1.19	1.16	1.19
Total	99.16	97.90	99.14	99.68	98.86
Number of O	21.5	21.5	21.5	21.5	21.5
Si	3.75	3.81	3.80	3.73	3.87
Ti	0.02	0.01	0.00	0.01	0.00
Al	6.48	6.46	6.46	6.54	6.30
Cr	0.02	0.01	0.02	0.01	0.02
B	0.34	0.35	0.36	0.41	0.45
Fe	0.74	0.66	0.72	0.70	0.70
Mn	0.02	0.02	0.02	0.04	0.03
Mg	2.92	2.92	2.90	2.84	2.86
Ca	0.01	0.01	0.01	0.01	0.01
Ba	0.00	0.00	0.00	0.00	0.00
Ni	0.00	0.00	0.00	0.00	0.00
Na	0.00	0.02	0.01	0.00	0.01
K	0.00	0.00	0.00	0.00	0.00
F	0.00	0.01	0.00	0.03	0.00
Cl	0.00	0.00	0.00	0.00	0.00
OH	1.00	0.99	1.00	0.97	1.00
Total cation	14.31	14.27	14.29	14.28	14.25
Mg/(Fe + Mg)	0.80	0.82	0.80	0.80	0.80
$\delta^{11}B_{NIST951}$‰	−9.8	−8.1	−8.1	−7.7	−6.1
±1σ‰	0.29	0.34	0.46	0.32	0.21

n.d., not determined. All Fe as FeO.

below based on these new B isotope data.

The prograde tourmaline is included as rounded to irregularly-shaped grains, which led Kawakami et al. (2008) to interpret these tourmaline grains as the precursors to kornerupine. The following reaction was proposed:

Tur + sodic Pl (An34) + Spr + Spl
--> Krn + Crn + calcic Pl (An82) + (fluid or melt) (1).

In the present study, the prograde tourmaline in sample TK2002122104 yielded an average $\delta^{11}B_{Tur}$ of −1.3 ±

Table 2. Summary of major element and B isotope compositions of tourmaline

Sample name	TK2002122104						
Spot no.	Tur1a	Tur1b	Tur1c	Tur2b	Tur3	Tur4	Tur5
Comment	Pro	Pro	Pro Rim	Pro	Pro	Pro	Pro in Crn
SiO_2	36.25	36.55	36.29	36.08	36.28	36.43	36.18
TiO_2	0.59	0.20	0.62	0.51	0.53	0.79	0.48
Al_2O_3	32.26	32.08	32.12	32.16	32.00	31.91	32.49
Cr_2O_3	0.32	0.26	0.65	0.14	0.71	0.21	0.50
B_2O_3 analyzed	10.10	10.13	10.21	10.18	10.11	10.26	10.29
B_2O_3 calc.*	10.51	10.54	10.46	10.50	10.48	10.52	10.57
FeO	3.45	3.54	3.27	3.43	3.11	3.35	3.47
MnO	0.06	0.08	0.00	0.00	0.07	0.01	0.00
MgO	8.60	8.87	8.33	8.93	8.60	8.83	8.82
CaO	2.02	2.11	2.09	2.06	2.18	2.06	1.84
BaO	0.08	0.08	0.00	0.02	0.08	0.00	0.00
Na_2O	1.70	1.56	1.58	1.69	1.59	1.64	1.74
K_2O	0.04	0.01	0.01	0.01	0.03	0.05	0.04
F	0.00	0.00	0.00	0.00	0.00	0.00	0.00
Cl	0.00	0.00	0.00	0.00	0.00	0.00	0.00
H_2O calc.	3.62	3.63	3.61	3.62	3.61	3.63	3.65
-O≡F	0.00	0.00	0.00	0.00	0.00	0.00	0.00
-O≡Cl	0.00	0.00	0.00	0.00	0.00	0.00	0.00
Total	99.09	99.11	98.77	98.81	98.92	99.15	99.49
Atomic proportions based on 15 cations exclusive of B, Na, K, Ca, and Ba (a.p.f.u.)							
B	3.00	3.00	3.00	3.00	3.00	3.00	3.00
Si	5.99	6.03	6.03	5.97	6.02	6.02	5.95
Al(IV)	0.01	0.00	0.00	0.03	0.00	0.00	0.05
Al(Z)	6.00	6.00	6.00	6.00	6.00	6.00	6.00
Al(Y)	0.28	0.24	0.29	0.24	0.26	0.22	0.24
Cr	0.04	0.03	0.08	0.02	0.09	0.03	0.06
Ti	0.07	0.02	0.08	0.06	0.07	0.10	0.06
Fe^{2+}	0.48	0.49	0.45	0.47	0.43	0.46	0.48
Mg	2.12	2.18	2.06	2.20	2.13	2.17	2.16
Mn	0.01	0.01	0.00	0.00	0.01	0.00	0.00
Ca	0.36	0.37	0.37	0.37	0.39	0.36	0.32
Na	0.55	0.50	0.51	0.54	0.51	0.52	0.55
K	0.01	0.00	0.00	0.00	0.01	0.01	0.01
Ba	0.01	0.01	0.00	0.00	0.01	0.00	0.00
X-site vacancy	0.08	0.12	0.12	0.09	0.09	0.10	0.11
F	0.00	0.00	0.00	0.00	0.00	0.00	0.00
Cl	0.00	0.00	0.00	0.00	0.00	0.00	0.00
OH	4.00	4.00	4.00	4.00	4.00	4.00	4.00
$Mg/(Fe^{2+} + Mg)$	0.82	0.82	0.82	0.82	0.83	0.82	0.82
$Ca/(Na + Ca + K + Ba)$	0.59	0.57	0.58	0.59	0.56	0.58	0.62
$\delta^{11}B_{NIST951}$	−2.0	−2.1	0.6	−1.4	−0.8	−1.7	−1.8
±‰	0.34	0.28	0.28	0.24	0.34	0.26	0.21

n.d., not determined. All Fe as FeO. *Boron calculated by stoichiometry (3 boron a.p.f.u.).

Table 2. (Continued)

Sample name	TK2002122104					
Spot no.	Tur6a	Tur6b	Tur7a	Tur7b	Tur8	Tur9
Comment	Retro	Retro	Retro	Retro	Retro	Retro
SiO_2	37.81	38.54	38.33	38.31	37.85	37.98
TiO_2	0.28	0.20	0.11	0.00	0.03	0.11
Al_2O_3	32.81	32.98	33.25	33.07	33.98	33.24
Cr_2O_3	0.02	0.05	0.18	0.02	0.08	0.16
B_2O_3 analyzed	9.98	9.20	9.32	9.77	9.89	10.13
B_2O_3 calc.*	10.66	10.60	10.71	10.69	10.71	10.61
FeO	3.79	3.51	3.22	2.70	2.94	3.35
MnO	0.03	0.03	0.00	0.00	0.00	0.00
MgO	8.10	7.36	8.05	8.53	8.06	7.64
CaO	0.36	0.34	0.22	0.08	0.16	0.25
BaO	0.00	0.07	0.00	0.02	0.07	0.00
Na_2O	2.24	2.25	2.16	2.11	2.24	2.30
K_2O	0.00	1.16	0.02	0.00	0.03	0.02
F	0.00	0.00	0.00	0.00	0.06	0.03
Cl	0.01	0.00	0.01	0.01	0.00	0.00
H_2O calc.	3.67	3.66	3.69	3.68	3.66	3.64
-O≡F	0.00	0.00	0.00	0.00	0.02	0.01
-O≡Cl	0.00	0.00	0.00	0.00	0.00	0.00
Total	99.10	99.35	98.55	98.30	99.01	98.82
Atomic proportions based on 15 cations exclusive of B, Na, K, Ca, and Ba (a.p.f.u.)						
B	3.00	3.00	3.00	3.00	3.00	3.00
Si	6.17	6.32	6.22	6.23	6.14	6.22
Al(IV)	0.00	0.00	0.00	0.00	0.00	0.00
Al(Z)	6.00	6.00	6.00	6.00	6.00	6.00
Al(Y)	0.31	0.37	0.36	0.34	0.50	0.42
Cr	0.00	0.01	0.02	0.00	0.01	0.02
Ti	0.03	0.02	0.01	0.00	0.00	0.01
Fe^{2+}	0.52	0.48	0.44	0.37	0.40	0.46
Mg	1.97	1.80	1.95	2.07	1.95	1.87
Mn	0.00	0.00	0.00	0.00	0.00	0.00
Ca	0.06	0.06	0.04	0.01	0.03	0.04
Na	0.71	0.71	0.68	0.67	0.70	0.73
K	0.00	0.24	0.00	0.00	0.01	0.00
Ba	0.00	0.00	0.00	0.00	0.00	0.00
X-site vacancy	0.23	0.00	0.28	0.32	0.26	0.22
F	0.00	0.00	0.00	0.00	0.03	0.01
Cl	0.00	0.00	0.00	0.00	0.00	0.00
OH	4.00	4.00	4.00	4.00	3.97	3.99
$Mg/(Fe^{2+} + Mg)$	0.79	0.79	0.82	0.85	0.83	0.80
Ca/(Na + Ca + K + Ba)	0.92	0.70	0.94	0.98	0.95	0.94
$\delta^{11}B_{NIST951}$	−3.7	−4.6	−3.9	−3.7	−4.5	−4.1
±‰	0.34	0.24	0.30	0.19	0.21	0.29

n.d., not determined. All Fe as FeO. *Boron calculated by stoichiometry (3 boron a.p.f.u.).

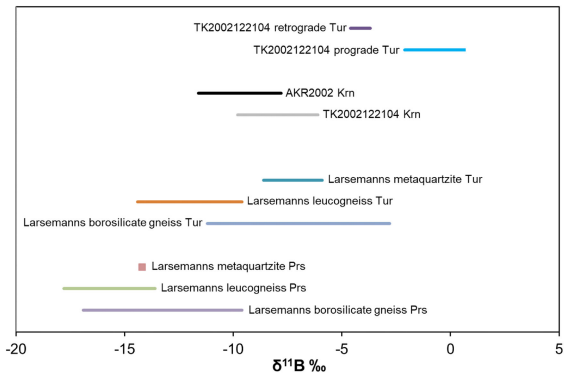

Figure 3. Ranges of boron isotope composition of the borosilicate minerals by rock type for the Larsemann Hills (MacGregor et al., 2013) and Akarui Point.

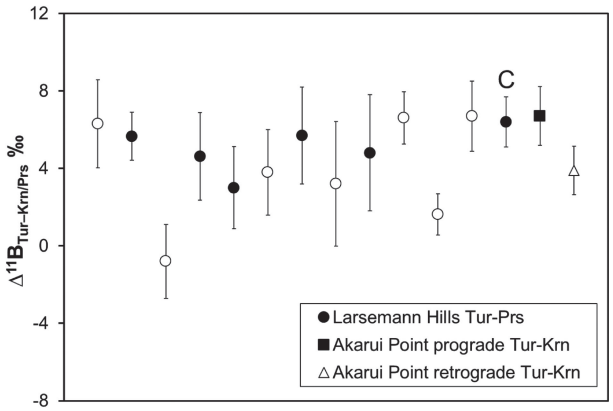

Figure 4. Plot of $\Delta^{11}B_{Tur\text{-}Krn/Prs}$ (= $\delta^{11}B_{Tur} - \delta^{11}B_{Krn/Prs}$). Larsemann Hills data are from MacGregor et al. (2013). Filled symbols, distribution of B isotopes is inferred to be equilibrium; unfilled symbols, distribution is not considered equilibrium. C, calculated fractionation (MacGregor et al., 2013).

0.9‰ (average ± 1σ), and the kornerupine enclosing the prograde tourmaline an average $\delta^{11}B_{Krn}$ of −8.0 ± 1.2‰. Therefore, $\Delta^{11}B_{Tur\text{-}Krn}$ of the average prograde tourmaline and average host kornerupine is +6.7 ± 1.5‰. This value does not appear to be influenced by post-entrapment B isotopic re-equilibration between prograde tourmaline and the host kornerupine because the prograde tourmaline included in corundum, which is protected from B isotopic re-equilibration, shows the same B isotopic value as the prograde tourmaline directly included within kornerupine. MacGregor et al. (2013) determined the B isotope distribution between prismatine and tourmaline under granulite facies conditions using a paragneiss containing tourmaline, grandidierite and prismatine from Larsemann Hills, Prydz Bay, East Antarctica (Fig. 3). In their study, prismatine systematically gave lower $\delta^{11}B$ values than coexisting tourmaline, and the measured $\Delta^{11}B_{Tur\text{-}Prs}$ (= $\delta^{11}B_{Tur} - \delta^{11}B_{Prs}$) = +5.0 ± 1.4‰ was considered to represent an equilibrium B isotope distribution (Fig. 4). Ab initio calculations following the method developed by Kowalski and Jahn (2011) and Kowalski et al. (2013) at 1000 K gives a B isotope fractionation factor of +6.4‰ (MacGregor et al., 2013). Based on these criteria, the kornerupine and prograde tourmaline in this study can be interpreted as isotopically in equilibrium within uncertainty (Fig. 4). Therefore, in a revision to the interpretation of Kawakami et al. (2008) that the prograde tourmaline was a precursor of kornerupine, we consider that the inclusion tourmalines within kornerupine and corundum formed in equilibrium with kornerupine under high-grade metamorphic conditions.

Since the formation of kornerupine and tourmaline in the initially B-poor mafic to ultramafic metamorphic rocks needs external input of B, we consider that the infiltration of a B-bearing fluid is required to form the Akarui Krn-Pl-Crn lens. As kornerupine at the Akarui Point is estimated to have formed at least at 800 °C (Kawakami et al., 2008), B isotopic fractionation between fluid and the prograde tourmaline is negligible according to the isotopic fractionation determined by Meyer et al. (2008). Therefore, the B isotope composition of the prograde tourmaline present within kornerupine is likely to represent that of the B-bearing fluid (i.e., $\delta^{11}B_{Fluid}$ = −1.3 ± 0.9‰). In contrast, $\Delta^{11}B_{Tur\text{-}Krn}$ is calculated to be +3.9 ± 1.3‰ between the average secondary tourmaline ($\delta^{11}B_{Tur}$ = −4.1 ± 0.4‰) and the average kornerupine ($\delta^{11}B_{Krn}$ of −8.0 ± 1.2‰) in TK2002122104 (Fig. 4). In other words, $\delta^{11}B$ is lower in secondary tourmaline than in prograde tourmaline because the secondary tourmaline crystallized at a lower temperature. It might be considered possible, given its similarity to the tourmaline-prismatine equilibrium value of $\Delta^{11}B_{Tur\text{-}Prs}$ = +5.0 ± 1.4‰ (MacGregor et al., 2013), that this might represent isotopic equilibrium instead. However, the presence of andalusite in the tourmaline-bearing microstructures replacing kornerupine shows that secondary tourmaline growth took place within the andalusite stability field, at lower pressures and temperatures than the stability field of kornerupine (e.g., Werding and Schreyer, 1996). Abundant secondary fluid inclusions occurring together with secondary tourmaline and other secondary minerals in TK2002122104 are consistent with estimates of ~ 500 °C for the retrograde fluid infiltration (Kawakami et al., 2008). Based on Meyer et al. (2008), $\Delta^{11}B_{Tur\text{-}fluid}$ at 500 °C is estimated to be ~ −1.9‰. Therefore, $\delta^{11}B_{fluid}$ of the fluid that formed secondary tourmaline under low-*P* greenschist facies conditions is calculated as ~ −2.2‰, essentially the same value as the core of prograde tourmaline. This suggests the fluid that formed secondary tourmaline had almost the same B isotope composition as the fluid that equilibrated with kornerupine and prograde tourmaline, and hence it is not necessary to in-

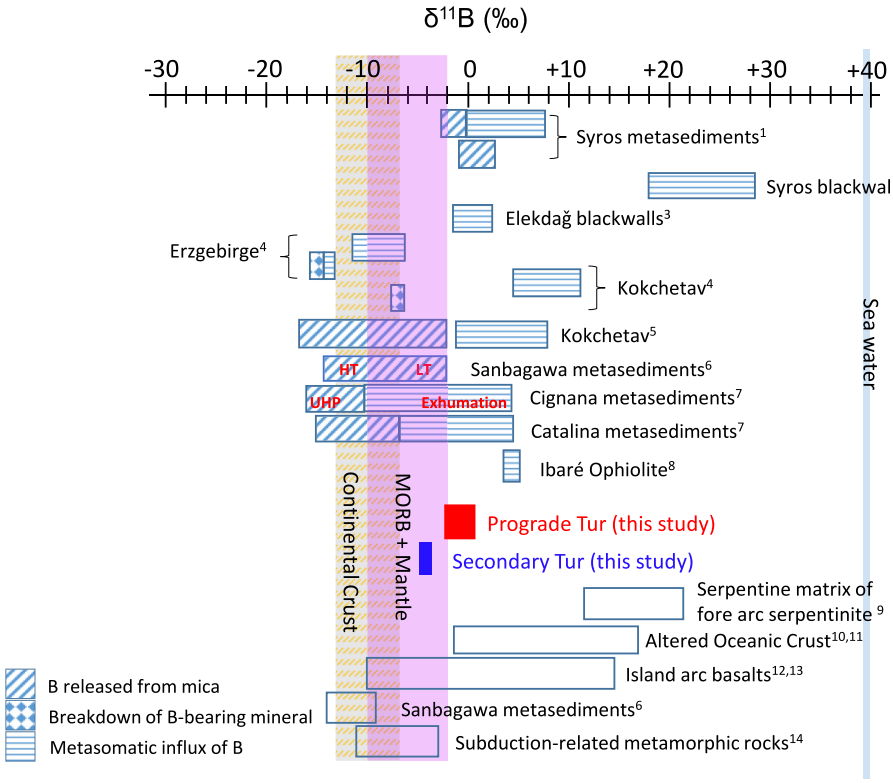

Figure 5. Boron isotopic compositions of tourmaline of this study in comparison with other metamorphic/metasomatic tourmaline and selected whole-rock B isotope compositions. Modified after Marschall et al. (2009). Data sources: [1]Marschall et al. (2008), [2]Marschall et al. (2006), [3]Altherr et al. (2004), [4]Marschall et al. (2009), [5]Ota et al. (2008), [6]Nakano and Nakamura (2001), [7]Bebout and Nakamura (2003), [8]Arena et al. (2020), [9]Benton et al. (2001), [10]Ishikawa and Nakamura (1992), [11]Smith et al. (1995), [12]Ishikawa and Nakamura (1994), [13]Ishikawa and Tera (1997), [14]Peacock and Hervig (1999).

voke the introduction of additional B-bearing fluid to explain the crystallization of secondary tourmaline.

Tourmaline in subduction zone metasediments (Sanbagawa, Catalina, and Lago di Cignana) formed by using B released from muscovite commonly show $\delta^{11}B$ values around −10‰ (Nakano and Nakamura, 2001; Bebout and Nakamura, 2003; Marschall et al., 2009; Fig. 5). Therefore, $\delta^{11}B$ values of the prograde tourmaline of this study (−1.3 ± 0.9‰) cannot be explained by the sediment-sourced fluid infiltration. Moreover, the $\delta^{11}B$ for prograde tourmaline is significantly lower than the $\delta^{11}B$ for seawater, which is therefore unlikely as a source of the fluid. In contrast, the $\delta^{11}B$ values of prograde tourmaline are between whole rock $\delta^{11}B$ of MORB and mantle rocks and of some sedimentary rocks, and are similar to the $\delta^{11}B$ of blackwall tourmalines that have been considered to have formed during decompression from high-*P* metamorphism (e.g., Altherr et al., 2004; Marocchi et al., 2011; van Hinsberg et al., 2011; Fig. 5). Therefore, a B-bearing fluid related to oceanic plate subduction and subsequent decompression may be a possible source of the B required to form the Krn-Pl-Crn lens. The dominance of kornerupine at the boundary between host gneiss and the lens (Kawakami et al., 2008) suggests that the B-bearing fluid infiltrated only after lens formation during the Late Proterozoic to Cambrian metamorphism. It is considered likely that this syn-metamorphic fluid may, therefore, have been sourced from a mixtures of mafic to ultramafic lithologies and sedimentary rocks in a subduction setting that preceded the collisional high-*T* metamorphism now preserved at Akarui Point and in the LHC in general.

Based on detailed geochemical study of its metabasic and meta-ultramafic rocks, Suda et al. (2008) concluded that LHC is an assembly of tectonic blocks or terranes of different origins. These blocks were composed of rocks derived from active crustal growth during Mesoproterozoic time and older rocks derived from Paleoproterozoic to Archaean cratons and oceanic crust. The blocks were considered to have amalgamated through multiple subductions of Pan-African and/or pre-Pan-African age (Suda et al., 2008). This view is consistent with the recent results of a regional study of inherited zircon ages (Dunkley et al., 2020) in that LHC is composed of suites of different origin, in which geological subdivisions based on protolith ages are proposed: the Innhovde Suite (1070–1040 Ma), the Rundvågshetta Suite (2520–2470 Ma), the Skallevikshalsen Suite (1830–1790 Ma), the Langhovde Suite (1100–1050 Ma), the East Ongul Suite (630 Ma), and the Akarui Suite (970–800 Ma). Although Akarui Point is located within the Akarui Suite, a boundary between positive and negative magnetic anomalies is indicated near Akarui Point in the reduced to the pole magnetic anomaly map of the LHC (Nogi et al., 2013), which would be consistent with the presence

of small tectonic discontinuity. Therefore, the metabasic and meta-ultramafic lenses found in Akarui Point may be the remnant of a mixing zone associated with an Ediacaran to Cambrian subduction channel within which B from multiple sources has been generated and mixed to produce a B-bearing fluid that interacted with the B-poor mafic to ultramafic rocks under high-*T* conditions.

ACKNOWLEDGMENTS

Dr. Cees-Jan de Hoog, of the Edinburgh Ion Microprobe Facility (EIMF) is thanked for setting up the B isotope analysis protocols and advising on initial data reduction. We are grateful to Prof. Edward Grew and an anonymous reviewer for constructive reviews and Prof. Tomokazu Hokada for editorial efforts. This study was financially supported by JSPS KAKENHI Grant numbers JP26400513 and JP19H01991 to T. Kawakami.

REFERENCES

Altherr, R., Topuz, G., Marschall, H., Zack, T. and Ludwig, T. (2004) Evolution of a tourmaline-bearing lawsonite eclogite from the Elekdağ area (Central Pontides, N Turkey): Evidence for infiltration of slab-derived B-rich fluids during exhumation. Contributions to Mineralogy and Petrology, 148, 409-425.

Arena, K.D.R., Hartmann, L.A., Lana, C.D.C., Queiroga, G.N. and Castro, M.P.De. (2020) Geochemistry and δ11B evolution of tourmaline from tourmalinite as a record of oceanic crust in the Tonian Ibaré ophiolite, Southern Brasiliano Orogen. Anais Da Academia Brasileira de Ciencias, 92, 1-16.

Baba, S., Horie, K., Hokada, T., Takehara, M., et al. (2022) Newly found Tonian metamorphism in Akebono Rock, eastern Dronning Maud Land, East Antarctica. Gondwana Research, 105, 243-261.

Bebout, G.E. and Nakamura, E. (2003) Record in metamorphic tourmalines of subduction-zone devolatilization and boron cycling. Geology, 31, 407-410.

Benton, L.D., Ryan, J.G. and Tera, F. (2001) Boron isotope systematics of slab fluids as inferred from a serpentine seamount, Mariana forearc. Earth and Planetary Science Letters, 187, 273-282.

Catanzaro, E.J., Champion, C.E., Garner, E.L., Marinenko, G., et al. (1970) Standard reference materials: Boric acid; isotopic, and assay standard reference materials. In NBS Special Publication 260-17. pp. 70, National Bureau of Standards, Boulder.

Dunkley, D.J., Hokada, T., Shiraishi, K., Hiroi, Y., et al. (2020) Geological subdivision of the Lützow-Holm Complex in East Antarctica: From the Neoarchean to the Neoproterozoic. Polar Science, 26, 100606.

Dutrow, B.L. and Henry, D.J. (2011) Tourmaline: A geologic DVD. Elements, 7, 301-306.

Grew, E.S. (1996) Borosilicates (exclusive of tourmaline) and Boron in rock-forming minerals in metamorphic environments. Reviews in Mineralogy, 33, 387-502. (Additions were made in 2002.)

Grew, E.S., Dymek, R.F., De Hoog, J.C.M., Harley, S.L., et al. (2015) Boron isotopes in tourmaline from the ca. 3.7-3.8 Ga Isua supracrustal belt, Greenland: Sources for boron in Eoarchean continental crust and seawater. Geochimica et Cosmochimica Acta, 163, 156-177.

Grew, E.S., Hystad, G., Hazen, R.M., Golden, J., et al. (2017) How many boron minerals occur in Earth's upper crust? Invited Centennial Paper, American Mineralogist, 102, 1573-1587.

Hiroi, Y., Shiraishi, K., Yanai, K. and Kizaki, K. (1983) Aluminum silicates in the Prince Olav and Soya Coasts, East Antarctica. Memoirs of National Institute for Polar Research, Special Issue, 28, 115-131.

Hiroi, Y., Shiraishi, K. and Motoyoshi, Y. (1991) Late Proterozoic paired metamorphic complexes in East Antarctica, with special reference to the tectonic significance of ultramafic rocks. In Geological Evolution of Antarctica (Thomson, M.R.A., Crane, J.A. and Thomson, J.W. Eds.). pp. 722, Cambridge University Press, Cambridge, 83-87.

Ishikawa, M., Motoyoshi, Y., Fraser, G.L. and Kawasaki, T. (1994) Structural evolution of Rundvågshetta region, Lützow-Holm Bay, East Antarctica. Proceedings of the NIPR Symposium on Antarctic Geosciences, 7, 69-89.

Ishikawa, T. and Nakamura, E. (1992) Boron isotope geochemistry of the oceanic crust from DSDP/ODP Hole 504B. Geochimica et Cosmochimica Acta, 56, 1633-1639.

Ishikawa, T. and Nakamura, E. (1994) Origin of the slab component in arc lavas from across-arc variation of B and Pb isotopes. Nature, 370, 205-208.

Ishikawa, T. and Tera, F. (1997) Source, composition and distribution of the fluid in the Kurile mantle wedge: Constraints from across-arc variations of B/Nb and B isotopes. Earth and Planetary Science Letters, 152, 123-138.

Iwamura, S., Tsunogae, T., Kato, M., Koizumi, T. and Dunkley, D.J. (2013) Petrology and phase equilibrium modeling of spinel-sapphirine bearing mafic granulite from Akarui point, Lützow-Holm complex, East Antarctica: Implications for the *P-T* path. Journal of Mineralogical and Petrological Sciences, 108, 345-350.

Kawakami, T. (2001) Tourmaline breakdown in the migmatite zone of the Ryoke metamorphic belt, SW Japan. Journal of Metamorphic Geology, 19, 61-75.

Kawakami, T. and Motoyoshi, Y. (2004) Timing of attainment of the spinel + quartz coexistence in garnet-sillimanite leucogneiss from Skallevikshalsen, Lützow-Holm Complex, East Antarctica. Journal of Mineralogical and Petrological Sciences, 99, 311-319.

Kawakami, T., Grew, E.S., Motoyoshi, Y., Shearer, C.K., et al. (2008) Kornerupine sensu stricto associated with mafic and ultramafic rocks in the Lützow-Holm Complex at Akarui Point, East Antarctica: What is the source of boron? In Geodynamic Evolution of East Antarctica: A Key to the East-West Gondwana Connection (Satish-Kumar, M., Motoyoshi, Y., Osanai, Y., Hiroi, Y. and Shiraishi, K. Eds.). pp. 456, Geological Society, London, Special Publications, 308, 351-375.

Kawakami, T., Hokada, T., Sakata, S. and Hirata, T. (2016) Possible polymetamorphism and brine infiltration recorded in the garnet-sillimanite gneiss, Skallevikshalsen, Lützow-Holm Complex, east Antarctica. Journal of Mineralogical and Petrological Sciences, 111, 129-143.

Kawakami, T., Sakai, H. and Sato, K. (2019) Syn-metamorphic B-bearing fluid infiltrations deduced from tourmaline in the Main Central Thrust zone, Eastern Nepal Himalayas. Lithos,

348–349.

Kitano, I., Hokada, T., Baba, S., Kamei, A., et al. (2021) U–Pb zircon geochronology of high-grade metamorphic rocks from outcrops along the Prince Olav Coast, East Antarctica. Program and Abstracts of the 12th Symposium on Polar Science, OGo2.

Kowalski, P.M. and Jahn, S. (2011) Prediction of equilibrium Li isotope fractionation between minerals and aqueous solutions at high P and T: an efficient ab initio approach. Geochimica et Cosmochimica Acta, 75, 6112–6123.

Kowalski, P.M., Wunder, B. and Jahn, S. (2013) Ab initio prediction of equilibrium boron isotope fractionation between minerals and aqueous fluids at high *P* and *T*. Geochimica et Cosmochimica Acta, 101, 285–301.

Krosse, S. (1995) Hochdrucksynthese, Stabilität und Eigenschaften der Borsilikate Dravit und Kornerupin sowie Darstellung und Stabilitätsverhalten eines neuen Mg–Al–Borates. Doctor's thesis, Ruhr–Universität, Bochum.

Leeman, W.P. and Sisson, V.B. (1996) Geochemistry of boron and its implications for crustal and mantle processes. Reviews in Mineralogy, 33, 644–707.

Leeman, W.P. and Tonarini, S. (2001) Boron isotopic analysis of proposed borosilicate mineral reference samples. Geostandards Newsletter, 25, 399–403.

MacGregor, J.R., Grew, E.S., De Hoog, J.C.M., Harley, S.L., et al. (2013) Boron isotopic composition of tourmaline, prismatine, and grandidierite from granulite facies paragneisses in the Larsemann Hills, Prydz Bay, East Antarctica: Evidence for a non-marine evaporite source. Geochimica et Cosmochimica Acta, 123, 261–283.

Marocchi, M., Marschall, H.R., Konzett, J., Tropper, P., et al. (2011) Metasomatic tourmaline in hybrid contact-bands between gneiss and peridotite in the Ulten Zone of the Eastern Italian Alps: Chemistry and boron isotopic composition. Canadian Mineralogist, 49, 245–261.

Marschall, H.R., Ludwig, T., Altherr, R., Kalt, A. and Tonarini, S. (2006) Syros metasomatic tourmaline: Evidence for very high-δ11 B fluids in subduction zones. Journal of Petrology, 47, 1915–1942.

Marschall, H.R., Altherr, R., Kalt, A. and Ludwig, T. (2008) Detrital, metamorphic and metasomatic tourmaline in high-pressure metasediments from Syros (Greece): Intra-grain boron isotope patterns determined by secondary-ion mass spectrometry. Contributions to Mineralogy and Petrology, 155, 703–717.

Marschall, H.R., Korsakov, A.V., Luvizotto, G.L., Nasdala, L. and Ludwig, T. (2009) On the occurrence and boron isotopic composition of tourmaline in (ultra)high-pressure metamorphic rocks. Journal of the Geological Society, 166, 811–823.

Meyer, C., Wunder, B., Meixner, A., Romer, R.L. and Heinrich, W. (2008) Boron-isotope fractionation between tourmaline and fluid: An experimental re-investigation. Contributions to Mineralogy and Petrology, 156, 259–267.

Mori, Y., Hokada, T., Miyamoto, T. and Ikeda, T. (2023) Metamorphic age and pressure-temperature conditions recorded in a sillimanite-garnet-bearing pelitic gneiss from Niban-nishi Rock of Niban Rock on the Prince Olav Coast, eastern Dronning Maud Land, East Antarctica: Evidence for Tonian metamorphism. Journal of Mineralogical and Petrological Sciences, 118, in press.

Motoyoshi, Y. and Ishikawa, M. (1997) Metamorphic and structural evolution of granulites from Rundvågshetta, Lützow-Holm Bay, East Antarctica. In The Antarctic Region: Geological Evolution and Processes (Ricci, C.A. Ed.). Terra Antarctica Publication, Siena, 65–72.

Nakamura, A., Kitamura, M. and Kawakami, T. (2014) Microstructural records of multiple retrograde local H_2O supplement in the pelitic gneiss, Lützow-Holm Complex at Akarui Point, East Antarctica. Mineralogy and Petrology, 108, 177–186.

Nakano, T. and Nakamura, E. (2001) Boron isotope geochemistry of metasedimentary rocks and tourmalines in a subduction zone metamorphic suite. Physics of the Earth and Planetary Interiors, 127, 233–252.

Nogi, Y., Jokat, W., Kitada, K. and Steinhage, D. (2013) Geological structures inferred from airborne geophysical surveys around Lützow-Holm Bay, East Antarctica. Precambrian Research, 234, 279–287.

Ota, T., Kobayashi, K., Kunihiro, T. and Nakamura, E. (2008). Boron cycling by subducted lithosphere; insights from diamondiferous tourmaline from the Kokchetav ultrahigh-pressure metamorphic belt. Geochimica et Cosmochimica Acta, 72, 3531–3541.

Peacock, S.M. and Hervig, R.L. (1999) Boron isotopic composition of subduction-zone metamorphic rocks. Chemical Geology, 160, 281–290.

Robbins, C.R. and Yoder, H.S. Jr. (1962) Stability relations of dravite, a tourmaline. Carnegie Institution Washington Yearbook, 61, 106–107.

Satish-Kumar, M., Hokada, T., Kawakami, T. and Dunkley, D.J. (2008) Geosciences research in East Antarctica (0°E–60°E): Present status and future perspectives. In Geodynamic Evolution of East Antarctica: A Key to the East-West Gondwana Connection (Satish-Kumar, M., Motoyoshi, Y., Osanai, Y., Hiroi, Y. and Shiraishi, K. Eds.). pp. 456, Geological Society, London, Special Publications, 308, 1–20.

Shiraishi, K., Ellis, D.J., Hiroi, Y., Fanning, C.M., et al. (1994) Cambrian orogenic belt in East Antarctica and Sri Lanka: Implications for Gondwana Assembly. Journal of Geology, 102, 47–65.

Smith, H.J., Spivack, A.J., Staudigel, H. and Hart, S.R. (1995) The boron isotopic composition of altered oceanic crust. Chemical Geology, 126, 119–135.

Suda, Y., Kawano, Y., Yaxley, G., Korenaga, H. and Hiroi, Y. (2008) Magmatic evolution and tectonic setting of metabasites from Lützow-Holm Complex, East Antarctica. In Geodynamic Evolution of East Antarctica: A Key to the East-West Gondwana Connection (Satish-Kumar, M., Motoyoshi, Y., Osanai, Y., Hiroi, Y. and Shiraishi, K. Eds.). pp. 456, Geological Society, London, Special Publications, 308, 211–233.

Suzuki, K. and Kawakami, T. (2019) Metamorphic pressure-temperature conditions of the Lützow-Holm Complex of East Antarctica deduced from Zr-in-rutile geothermometer and Al_2SiO_5 minerals enclosed in garnet. Journal of Mineralogical and Petrological Sciences, 114, 267–279.

Van Hinsberg, V.J., Henry, D.J. and Marschall, H.R. (2011) Tourmaline: An ideal indicator of its host environment. Canadian Mineralogist, 49, 1–16.

Warr, L.N. (2021) IMA–CNMNC approved mineral symbols. Mineralogical Magazine, 85, 291–320.

Werding, G. and Schreyer, W. (1996) Experimental studies on borosilicates and selected borates. In Boron: Mineralogy, Petrology and Geochemistry (Anovitz, L.M. and Grew, E.S. Eds.). Mineralogical Society of America, Reviews in Mineralogy, 33, 117–163.

Yanai, K., Kizaki, K., Shiraishi, K., Hiroi, Y. and Kanisawa, S. (1984) Antarctic geological map series sheet 20, Akarui Point and Naga-iwa Rock. National Institute of Polar Research, Tokyo.

Yoshimura, Y., Motoyoshi, Y. and Miyamoto, T. (2008) Sapphirine + quartz association in garnet: implication for ultrahigh-temperature metamorphism at Rundvågshetta, Lützow-Holm Complex, East Antarctica. In Geodynamic Evolution of East Antarctica: A Key to the East-West Gondwana Connection (Satish-Kumar, M., Motoyoshi, Y., Osanai, Y., Hiroi, Y. and Shiraishi, K. Eds.). pp. 456, Geological Society, London, Special Publications, 308, 377-390.

Manuscript received January 31, 2023
Manuscript accepted April 16, 2023
Advance online publication April 25, 2023
Released online publication May 19, 2023
Manuscript handled by Tomokazu Hokada